HHS Public Access

Author manuscript

Neurobiol Dis. Author manuscript; available in PMC 2017 February 01.

Published in final edited form as:

Neurobiol Dis. 2016 February ; 86: 86–98. doi:10.1016/j.nbd.2015.11.008.

Pathogenesis of severe ataxia and tremor without the typical signs of neurodegeneration

Joshua J. White[1,2,4], **Marife Arancillo**[1,4], **Annesha King**[1,4], **Tao Lin**[1,4], **Lauren N. Miterko**[3,4], **Samrawit A. Gebre**[1,4], and **Roy V. Sillitoe**[1,2,3,4]

[1]Department of Pathology & Immunology, 1250 Moursund Street, Suite 1325, Houston, Texas 77030, USA

[2]Department of Neuroscience, 1250 Moursund Street, Suite 1325, Houston, Texas 77030, USA

[3]Program in Developmental Biology, Baylor College of Medicine, 1250 Moursund Street, Suite 1325, Houston, Texas 77030, USA

[4]Jan and Dan Duncan Neurological, Research Institute of Texas Children's Hospital, 1250 Moursund Street, Suite 1325, Houston, Texas 77030, USA

Abstract

Neurological diseases are especially devastating when they involve neurodegeneration. Neuronal destruction is widespread in cognitive disorders such as Alzheimer's and regionally localized in motor disorders such as Parkinson's, Huntington's, and ataxia. But, surprisingly, the onset and progression of these diseases can occur without neurodegeneration. To understand the origins of diseases that do not have an obvious neuropathology, we tested how loss of CAR8, a regulator of IP3R1-mediated Ca^{2+}-signaling, influences cerebellar circuit formation and neural function as movement deteriorates. We found that faulty molecular patterning, which shapes functional circuits called zones, leads to alterations in cerebellar wiring and Purkinje cell activity, but not to degeneration. Rescuing Purkinje cell function improved movement and reducing their Ca^{2+} influx eliminated ectopic zones. Our findings in *Car8*^{wdl} mutant mice unveil a pathophysiological mechanism that may operate broadly to impact motor and non-motor conditions that do not involve degeneration.

Keywords

ataxia; tremor; neurodegeneration; *in vivo* electrophysiology; behavior; cerebellum

Corresponding Author: Dr. Roy V. Sillitoe, **Tel:** 832-824-8913, **Fax:** 832-825-1251, sillitoe@bcm.edu.

Conflicts of interest: We have nothing to disclose.

INTRODUCTION

The severity of neurological disease increases with neurodegeneration. In Alzheimer's disease, cognition declines with widespread neuronal destruction and in Parkinson's, Huntington's, and ataxia movement rapidly deteriorates with the onset of neurodegeneration (Gennarino et al., 2015). However, neurodegeneration may not be a prerequisite for such dysfunction. Here, we used the cerebellum as a model to uncover how an intact circuit can still impact disease outcome.

The cerebellum is involved in a number of motor disorders including ataxia, dystonia, and tremor (Louis et al., 2011, Orr, 2012, Wilson and Hess, 2013). Purkinje cells are the presumed source of these disorders, and they often degenerate (Unno et al., 2012, Orr, 2012, Prudente et al., 2013, Louis, 2014). Yet in some diseases, movement is obstructed before Purkinje cells degenerate (Shakkottai et al., 2011). In other cases, motor problems start early in life before circuits mature, without leading to massive degeneration (Pandolfo, 2008). This raises a critical question; what features of Purkinje cell wiring influence motor disease when basic circuit anatomy persists?

To address this problem, we first needed to identify an appropriate model. We found that the spontaneous mutant mouse, *waddles*, may be ideal for several reasons. W*addles* (*wdl*) mice contain a deletion in exon 8 of the carbonic anhydrase 8 gene (*Car8*), creating a null allele with no protein (Jiao et al., 2005). In the brain, CAR8 protein is expressed predominantly in Purkinje cells. Its expression is initiated during embryogenesis and maintained into adulthood (Kato, 1990, Taniuchi et al., 2002). CAR8 belongs to a family of zinc metalloenzymes that catalyze the reversible hydration of CO_2 (Tripp et al., 2001), although it lacks the catalytic domain that would make it an active carbonic anhydrase (Kato, 1990). It does, however, bind to inositol 1,4,5-triphosphate receptor type 1 (IP_3R1), with the effect of decreasing the affinity of IP_3 for its receptor (Hirota et al., 2003). *Car8*^{wdl} mice have ataxia and appendicular dystonia, with cerebellar microcircuit abnormalities (Hirasawa et al., 2007) occurring without gross anatomical defects (Jiao et al., 2005). In humans, mutations in the homologous gene, *CA8*, also cause ataxia and a predisposition for quadrupedal locomotion (Turkmen et al., 2009). *CA8*, with at least three other ataxia/tremor causing genes, define this heterogeneous condition called CAMRQ (Ali et al., 2012). Interestingly, *ITPR1* mutations cause SCA15 spinocerebellar ataxia, which can also involve tremor (Van de Leemput et al., 2007). The pathogenic roles of *Car8* suggested to us that *Car8*^{wdl} mice could be useful for testing how motor diseases arise without neurodegeneration.

We tested how three major features of circuit connectivity impact ataxia pathogenesis and the progression of movement-associated tremor: zonal patterning, Purkinje cell firing, and Purkinje cell neurodegeneration. Two possibilities were that in *Car8*^{wdl}, ataxia and tremor are initiated by developmental defects, with motor deficits emerging consequently either because of neuronal misfiring or degeneration. To differentiate between these possibilities, we combined the *Car8*^{wdl} model with molecular zone analyses, neural tracing, *in vivo* electrophysiology, pharmacological manipulations, and behavioral paradigms. We

uncovered an unexpected role for cerebellar wiring during ataxia and tremor pathogenesis that does not involve degeneration or cell loss.

MATERIALS AND METHODS

Animals

Car8^{wdl} mutants (*wdl/wdl*) and C57BLKS/J controls were purchased from The Jackson Laboratory (Bar Harbor, ME) and then maintained in our animal colony under an approved IACUC animal protocol according to the institutional guidelines at Baylor College of Medicine.

Mouse perfusion and tissue procedures

The mice were perfused with 4% paraformaldehyde and the tissue cut on a cryostat. Immunohistochemistry, *in situ* hybridization, and neural tracing were carried out as described previously (White et al., 2014; see Supplemental Information).

Western blotting

For each blot, mutant and control cerebella from P30 mice were rapidly dissected and then placed in RIPA buffer containing protease inhibitors before homogenization. We then performed standard SDS polyacrylamide gel electrophoresis (Sillitoe et al., 2003).

Drug treatment

Chlorzoxazone (CHZ; Sigma, St Louis, MO, USA) was administered orally by adding the drug to the drinking water to make a 15 mM solution (Alvina and Khodakhah, 2010) and nimodipine (Sigma, St Louis, MO, USA) was given subcutaneously at a dosage of 5 ml/kg.

Behavioral analysis

Rotarod performance was quantified by recording the latency to fall or to rotate 3 consecutive times on an accelerating rod (White et al., 2014), and tremor amplitude and frequency were analyzed on a single trial with a Tremor Monitor (San Diego Instruments). Between-group differences were statistically evaluated by Student's t-test. Between-trial differences were statistically evaluated with repeated measures ANOVA.

In vivo electrophysiology

Mice were anesthetized with Ketamine/Dexmedetomidine (75 mg/kg and 0.5 mg/kg respectively) and maintained with ~0.15%–0.25% isoflurane (White et al., 2014). Single unit recordings were attained from Purkinje cells with 5–8 MΩ tungsten electrodes (Thomas Recording, Germany) and digitized into Spike2 (CED, England). Spike frequency, ISI CV, CV2, rhythm index, and oscillation frequency were computed and reported as mean ± standard error of the mean (SEM). Firing frequency is defined as the number of spikes over a predetermined period of a recording, CV is calculated as the ratio of the standard deviation (SD) of ISIs to the mean ISI of a given cell, CV2 ($= 2|ISI_{n+1} - ISI_n|/(ISI_{n+1} + ISI_n)$) measures firing pattern variability within a short period of two interspike intervals (Holt et al., 1996), and rhythm index is a measure of the strength of oscillating patterns within a given period.

Oscillation frequency was calculated as the inverse of the time lag of the first peak ($1/t_1$) on autocorrelograms of simple spike activity. Please refer to the Supplemental Information for more details on the electrophysiology methods and the types of spike analyses that were conducted. Statistical analyses were performed with unpaired, two-tailed Student's t-tests. Significance is indicated in the graphs for $p < 0.05$, $p < 0.01$ or $p < 0.001$ with *, **, and ***, respectively.

RESULTS

Movement and learning deteriorate over time and a severe tremor develops in *Car8^{wdl}*

Car8 mRNA and protein are highly localized to cerebellar Purkinje cells (Taniuchi et al., 2002, Lakkis et al., 1997a, Lakkis et al., 1997b) (Fig. 1; n = 6 mutants and 9 controls; Fig. S1, S2, S3). We therefore tested the extent to which the loss of CAR8 causes motor defects in juvenile, adult, and aged mice. Motor impairments were obvious between the second to third postnatal week when the *Car8^{wdl}* mice are learning to make independent movements (Movie S1, S2). We used the rotarod assay to test whether motor performance declines from juveniles at P30 through several adult ages and into aging. Indeed, as the mutant mice aged their motor performance worsened significantly whereas the aged control mice were able to perform to a similar level as younger controls (Fig. 2A). Notably, we found that, at all ages, *Car8^{wdl}* mutants performed poorly compared to their age-matched controls when we examined the performance trajectory to the fourth day of the rotarod paradigm (P30: control = 277.545 ± 12.524 s, *Car8^{wdl}* mutants = 134.969 ± 17.559 s, $p = 2.577\times10^{-30}$; P90: control = 285.042 ± 10.117 s, *Car8^{wdl}* mutants = 41.381 ± 11.207 s, $p = 1.244\times10^{-30}$; P360: control = 273.267 ± 5.066 s, *Car8^{wdl}* mutants = 15.519 ± 5.912 s, $p = 3.409\times10^{-27}$; Fig. 2A,B). Next, we wanted to test whether motor learning is defective in the *Car8^{wdl}* mouse. By comparing P30, P90, and P360 mice over multiple days and trials, we found that, in *Car8^{wdl}* mice, motor learning on the rotarod improves significantly at P30 but not over the 12 trials at P90 or P360 (P30 *Car8^{wdl}*: $F_{(11, 110)} = 3.437$, $p = 0.0004$; P90 *Car8^{wdl}*: $F_{(11, 66)} = 1.681$, $p = 0.0973$; P360 *Car8^{wdl}*: $F_{(11, 88)} = 0.4660$, $p = 0.9194$; Repeated measures, one-way ANOVA; Fig. 2). In addition to the disturbance in locomotion and motor learning, we observed that *Car8^{wdl}* mice shake uncontrollably (Movie S2, S3). We wondered whether this behavior might be indicative of a cerebellar-derived tremor as recent work indicates a strong dependence of tremor on the Purkinje cell circuit (Louis, 2014). To test this possibility, we used a Tremor Monitor to quantitatively measure the frequency and power of rhythmic, shaking movements. Typically, the peak of cerebellar action tremor occurs at a frequency between 4 and 14 Hz (Miwa, 2007, Park et al., 2010, Handforth, 2012). The tremor in control and *Car8^{wdl}* mice both occurred between 4 and 14 Hz. However, the peak tremor of *Car8^{wdl}* mice of all ages examined was of a lower frequency than the expected "physiological tremor" in controls (control: 12.487 ± 0.260 Hz; *Car8^{wdl}*: 9.237 ± 0.178; $p = 7.226\times10^{-19}$; Fig. 2) and they have a much higher power (control: $2.13\times10^{-4} \pm 1.567\times10^{-5}$; *Car8^{wdl}*: $7.52\times10^{-4} \pm 5.73\times10^{-5}$; $p = 4.233\times10^{-15}$; Fig. 2C). We then tested whether the tremor became more pronounced over time, and indeed, by comparing P30, P90, and P360 *Car8^{wdl}* mutants, we found that tremor amplitude increases, suggesting that tremor severity was sensitive to age (Fig. 2; P30 = $1.46\times10^{-4} \pm 3.319\times10^{-5}$; P90 = $6.42\times10^{-4} \pm 7.266\times10^{-5}$, P180 = $8.15\times10^{-4} \pm 9.891\times10^{-5}$; P360 = $1.41\times10^{-3} \pm 1.54\times10^{-4}$; $F_{(3, 76)} =$

26.75, $p < 0.0001$; Fig. 2C,D). But, interestingly, as tremor amplitude increases with age in *Car8*^{wdl} mutants, frequency decreases (Fig. 2; P30 = 10.5 ± 0.492 Hz; P90 = 9.48 ± 0.356 Hz, P180 = 9.05 ± 0.336 Hz; P360 = 8.176 ± 0.312 Hz; $F_{(3, 74)} = 5.639$, $p = 0.0016$; Fig. 2C) in a manner that is strikingly reminiscent of human essential tremor patients (Elble, 2000, Thanvi et al., 2006). Control mice do not show any difference in peak frequency across age (Control: P30 = 12.735 ± 0.489 Hz; P90 = 12.308 ± 0.458 Hz; P180 = 12.333 ± 0.624 Hz; P360 = 12.077 ± 0.399 Hz; $F_{(3, 65)} = 0.3001$, $p = 0.8252$; Fig. 2C). However, with age, there is an increase in amplitude of physiological tremor in control mice (P30 = 1.17×10^{-4} ± 1.089×10^{-5}; P90 = 2.39×10^{-4} ± 2.452×10^{-5}; P180 = 2.63×10^{-4} ± 3.053×10^{-5}; P360 = 3.85×10^{-4} ± 4.569×10^{-5}; $F_{(3, 65)} = 25.50$, $p < 0.0001$; Fig. 2), which is expected in normal aging. The shaking motion of *Car8*^{wdl} mice is thus consistent with an essential tremor. These tremors combined with the worsening of rotarod performance over time indicate that loss of CAR8 triggers a rotarod deficit plus a cerebellar, essential tremor-like phenotype that increases with age in the *Car8*^{wdl} mice. In order to understand how these early onset and progressive motor dysfunctions occur, we next examined the *Car8*^{wdl} mice for defects in cerebellar pathology and a gradual loss of neurons over time.

Car8^{wdl} mice do not exhibit cerebellar neurodegeneration or Purkinje cell loss with age

Neurodegenerative diseases can involve the regression and/or restructuring of neuronal dendrites and axons, deterioration of surrounding microcircuits, and the eventual death and loss of neurons. These defects often cause a change in gross morphology and a reduction in the size of the affected structure. We found that *Car8*^{wdl} mice, at all ages examined, have a normal gross cerebellar anatomy with intact patterning of the lobules into 10 individual folds (Fig. 3; Larsell, 1970). Next, we measured cerebellar cortical thickness based on combined fluorescent nissl plus calbindin immunostaining to detect potential degenerative changes in the Purkinje cell dendrites over time. Comparisons of cortical thickness between P30, P90, P180, and P360-P420 mice showed that except for P30 (control = 173.852 ± 5.259 μm; *Car8*^{wdl} = 153.760 ± 2.409 μm; $p = 9.82\times10^{-3}$), over time there was no dendritic degeneration in *Car8*^{wdl} mice as compared to controls, P90 (control = 169.665 ± 2.564 μm; *Car8*^{wdl} = 170.610 ± 2.473 μm; $p = 0.795$), P180 (control = 169.736 ± 2.012 μm; *Car8*^{wdl} = 168.037 ± 2.280 μm; $p = 0.583$) or P360–P420 (control = 168.737 ± 3.130 μm; *Car8*^{wdl} = 164.649 ± 1.939 μm; $p = 0.285$; Fig. 3). The observed difference in molecular layer thickness between mutants and controls at P30, but not at later ages, suggested a developmental delay. Indeed, when we looked at an earlier postnatal age (P15), we also found a significant difference between control and *Car8*^{wdl} (P15: control = 136.126 ± 3.203 μm; *Car8*^{wdl} = 118.251 ± 4.657 μm; $p = 6.62\times10^{-3}$). We next examined the mutant cerebella for cell loss. In degenerative ataxias, cell loss results in gaps in calbindin expression (Sarna et al., 2003). Examination of calbindin expression on sagittal sections cut through *Car8*^{wdl} and control cerebella revealed identical staining patterns, with the Purkinje cell somata forming a monolayer with no gaps (Fig. 3). These data demonstrate that *Car8*^{wdl} mice do not exhibit increased degeneration or cell loss above the typical levels seen in controls in juvenile, adult, and aged mice. Because of the lack of a degenerative pathology, we postulated that perhaps the motor problems reflect poor circuit wiring. This idea is supported by findings that *Car8*^{wdl} have a lower number of functional parallel fiber-Purkinje cell

synapses and an increased density and apical-basal distribution of VGLUT2-positive climbing fiber terminals (Hirasawa et al., 2007).

The patterning of the cerebellum into zones is spatially and temporally altered in *Car8*^{wdl}

The cerebellum is wired into functional modules called zones (Apps and Hawkes, 2009). Zones play a central role in cerebellar-associated diseases including metabolic disorders, stroke, and viral infection (Welsh et al., 2002, Sarna and Hawkes, 2003, Williams et al., 2007). We therefore hypothesized that altered zones could be involved in the *Car8*^{wdl} motor deficits. To test this, we examined the zonal relationship between zebrinII/aldolaseC (Brochu et al., 1990) and the small heat shock protein HSP25 (Armstrong et al., 2000). In control mice, by P15 zebrinII and HSP25 show minimal co-expression in limb proprioception circuits (Armstrong and Hawkes, 2000). In *Car8*^{wdl}, we found that HSP25 was heavily co-expressed in the same zones as zebrinII (Fig. 4A; n = 10). However, by P30 the HSP25 zones acquired their normal pattern in lobules VI/VII and IX/X (Fig. 4A; n = 5). But, double labeling with zebrinII and PLCβ4, which mark complementary zones in adults (Sarna et al., 2006), shows that the two patterns exhibited weak expression boundaries in the mutants (arrows Fig. 4B; n = 6). Wholemount analysis of an early zonal marker, the cystoskeletal protein neurofilament heavy chain (NFH; White and Sillitoe, 2013), further revealed that the boundaries in *Car8*^{wdl} are not sharply delineated because of poor sculpting (Fig. S4; n = 4). These data indicate that in *Car8*^{wdl}, zone development is delayed and the data also suggest that the assembly of the topographic map is spatially mispatterned. Therefore, we next tested if the zone defects impact sensory-motor circuit wiring by examining the trajectory and terminal field topography of cerebellar afferents.

The wiring of cerebellar sensory maps is poorly coordinated in *Car8*^{wdl} mice

Mossy fibers carry sensory signals to the cerebellum from more than three-dozen brainstem and spinal cord nuclei (Fu et al., 2011). Among these pathways is the spinocerebellar tract, which carries proprioceptive signals (Bosco and Poppele, 2001). Purkinje cell zones are thought to shape spinocerebellar wiring during postnatal development (Sotelo, 2004, Sillitoe et al., 2010, White et al., 2014). Because the loss of *Car8* alters zebrinII, we tested whether Purkinje cells alter the mossy fiber map in *Car8*^{wdl}. To test this, we injected WGA-Alexa 555 into the lower thoracic-upper lumbar spinal cord (Fig. S3) of adult P90 *Car8*^{wdl} mice (n = 6) and controls (n = 6) (Fig. 5A). The adult mutant spinocerebellar map is not sharply delineated, and reminiscent of the Purkinje cell zone defects (Fig. 4C). The topography of the afferent map was less clear at P90 compared to P30 (Fig. 5B; n = 4 controls and 3 mutants). Earlier injections at P4 and the tissue analyzed at P5 indicated that *Car8* is required for the formation of the mossy fiber map (Fig. 5D; n = 8 controls and 8 mutants). Injections at P2 and the analysis conducted at P3 revealed that despite the long-term defects in the organization, the fibers do enter the correct cerebellar lobules and therefore follow a relatively normal trajectory (Fig. 5D; n = 2 controls and 4 mutants).

To investigate how multiple functional sensory maps are spatially integrated in *Car8*^{wdl} mice, we also examined the topography of the cuneocerebellar tract. Cuneocerebellar mossy fibers carry proprioceptive and fine touch signals for the forelimbs, and they terminate in a near perfect complementary pattern to the spinocerebellar fibers (Gebre et al., 2012). To

resolve this relationship, we used the expression of VGLUT1, which labels cuneocerebellar terminals, and VGLUT2, which labels spinocerebellar terminals (Gebre et al., 2012). In P21 *Car8*^{wdl} mice, we did not find complementary circuit zones, but instead VGLUT1 and VGLUT2 expression were overlapping in a manner that reflected the altered relationship between the different subsets of Purkinje cell zone markers (asterisks Fig. 5E; n = 3 of each genotype). To examine if cerebellar function is affected we next asked whether changes in activity accompany the miswiring.

Purkinje cell activity is severely impaired in *Car8*^{wdl} mice

Slice physiology showed that *Car8*^{wdl} mice have a decrease in the frequency of mini excitatory postsynaptic currents (Hirasawa et al., 2007). To test whether these defects are translated into circuit level problems, we used an extracellular recording approach to measure Purkinje cell activity *in vivo* (White et al., 2014). Purkinje cells exhibit a specific firing profile that consists of simple spike (SS) action potentials, which are generated intrinsically and modulated by mossy fiber inputs and complex spike (CS) action potentials, which are triggered by climbing fibers. We found that SS firing frequency is not significantly different between control and *Car8*^{wdl} mice (control = 48.461 ± 4.407 Hz; *Car8*^{wdl} = 54.632 ± 3.901 Hz; p = 0.304, Fig. 6E). However, the pattern of firing is significantly altered. Compared to the controls, *Car8*^{wdl} Purkinje cells fire with long pauses (Fig. 6). The long SS pauses cause a significant increase in the CV of the ISI in *Car8*^{wdl} (control = 0.3198 ± 0.020; *Car8*^{wdl} = 1.3561 ± 0.174; p = 1.91×10^{-5}, Fig. 6H). However, examination of local regularity patterns via CV2 analysis and a rhythm index showed that while *Car8*^{wdl} Purkinje cells fire erratically on the whole, they also display rhythmic properties. *Car8*^{wdl} Purkinje cells have a lower CV2, suggesting higher regularity during firing (control = 0.318 ± 0.011; *Car8*^{wdl} = 0.252 ± 0.022; p = 0.0123; Fig. 6J). Rhythm index (Arancillo et al., 2015) analysis indicates a higher rhythmicity of *Car8*^{wdl} Purkinje cells compared to control cells (control = 0.958 ± 0.154; *Car8*^{wdl} = 1.807 ± 0.229; p = 0.005; Fig. 6). Oscillation frequency (Arancillo et al., 2015), however, was not significantly different (control = 62.083 ± 7.54; *Car8*^{wdl} = 80.112 ± 5.169; p = 0.062; Fig. 6) although it does trend toward an increase in *Car8*^{wdl}.

We next considered whether the pause free periods of firing have features that may be masked by the relatively long segments of quiescence. Interestingly, analysis of SS firing without the long pauses revealed periods of high frequency firing in *Car8*^{wdl} Purkinje cells. In addition to the higher rate compared to control cells, the mutant cells minus the long pauses had a lower CV that is comparable to controls (Fig. 7). In contrast, the CV2 of the mutant cells remained lower than control cells, with and without the long pauses (Fig. 7).

We next predicted that the abnormal properties of SS firing in *Car8*^{wdl} Purkinje cells could potentially lead to abnormal CS firing (White et al., 2014, Chen et al., 2010), because the circuit operates within a closed loop involving Purkinje cells, cerebellar nuclear neurons, inferior olive neurons, and finally their target Purkinje cells (Chaumont et al., 2013, Witter et al., 2013). Indeed, the CS firing frequency is significantly decreased in *Car8*^{wdl} mice (control = 1.017 ± 0.057 Hz; *Car8*^{wdl} = 0.591 ± 0.063 Hz; p = 3.318×10^{-5}, Fig. 6F), whereas the CS CV is not changed (control = 0.750 ± 0.0285; *Car8*^{wdl} = 0.690 ± 0.038; p =

0.217, Fig. 6I). But, the regularity of CS firing is altered as measured by CV2 (control = 0.953 ± 0.0345; *Car8*^{wdl} = 0.750 ± 0.027; p = 1.16×10^{-5}, Fig. 6K). We hypothesized that if the observed Purkinje cell firing defects underlie *Car8*^{wdl} ataxia, then correcting them should improve motor performance.

Chlorzoxazone corrects several properties of Purkinje cell firing in *Car8*^{wdl} mice

Feeding mice the FDA-approved muscle relaxant chlorzoxazone (CHZ) increases the probability of opening Ca^{2+}-dependent K^+ channels, which affects firing and improves motor performance in ataxic mice (Alvina and Khodakhah, 2010; Gao et al., 2012). We performed *in vivo* electrophysiology to assess the effects of CHZ treatment on *Car8*^{wdl} mice. We found that SS firing frequency is not significantly different between any of the conditions after 10 days of treatment (control untreated = 48.461 ± 4.407 Hz, control treated = 47.470 ± 3.970 Hz, p = 0.869; *Car8*^{wdl} untreated = 54.632 ± 3.901 Hz, p = 0.305; *Car8*^{wdl} treated = 51.413 ± 4.653 Hz, p = 0.601; Fig. 6E). The CV of SS firing is corrected in treated *Car8*^{wdl} mice (*Car8*^{wdl} untreated = 1.3561 ± 0.174; *Car8*^{wdl} treated = 0.418 ± 0.092; p = 6.15×10^{-5}; Fig. 6H) and is no longer significantly different from controls (control untreated = 0.3198 ± 0.020; *Car8*^{wdl} treated = 0.418 ± 0.092; p = 0.226; Fig. 6). CS frequency was significantly increased with treatment (*Car8*^{wdl} untreated = 0.591 ± 0.063 Hz; *Car8*^{wdl} treated = 0.850 ± 0.110 Hz; p = 0.019; Fig. 6F) and was no longer significantly different from controls (control untreated = 1.017 ± 0.057 Hz; *Car8*^{wdl} treated = 0.850 ± 0.110 Hz; p = 0.110; Fig. 6F). Note that there were no significant differences between untreated and treated controls in frequency and CV (SS frequency: control untreated = 48.461 ± 4.407 Hz; control treated = 47.470 ± 3.970 Hz; p = 0.869; SS CV: control untreated = 0.3198 ± 0.020; control treated = 0.3670 ± 0.0230; p = 0.134; CS frequency: control untreated = 1.017 ± 0.057 Hz; control treated = 0.970 ± 0.088 Hz; p = 0.657; CS CV: control untreated = 0.750 ± 0.028; control treated = 0.780 ± 0.020; p = 0.408; Fig. 6I). However, CHZ did not recover the mutant CV2 to control levels (*Car8*^{wdl} untreated = 0.252 ± 0.022; *Car8*^{wdl} treated = 0.261 ± 0.018; p = 0.749; Fig. 6K) or alter the CV2 in controls (control untreated = 0.318 ± 0.011; control treated = 0.339 ± 0.022; p = 0.411). Because CHZ corrects a number of the firing properties in *Car8*^{wdl} mice, we next asked whether this change is enough to affect movement and, if it is, to what extent is motor performance improved by the CHZ treatment.

CHZ treatment improves the motor performance of *Car8*^{wdl} mice

We provided CHZ to the mice in their drinking water and then used the accelerating rotarod paradigm to track motor behavior over time (n = 10 controls and 9 mutants). Before treatment, the control mice performed consistently and significantly better than the *Car8*^{wdl} mice (control = 267.6 ± 8.450 s; *Car8*^{wdl} = 44.156 ± 9.701 s; p = 7.437×10^{-190}; Fig. 5N,O; Movie S4). During treatment the control mice did not show a significant change in performance (control untreated = 267.6 ± 8.450 s; control treated = 269.305 ± 13.735 s; p = 0.689; Fig. 6N,O). In contrast, treated *Car8*^{wdl} improve significantly from their pre-treatment performance (*Car8*^{wdl} untreated = 44.156 ± 9.701; *Car8*^{wdl} treated = 68.411 ± 11.915; p = 3.957×10^{-08}; Fig. 6O; Movie S5). However, the rotarod performance of the *Car8*^{wdl} was not rescued to control levels (control treated = 269.305 ± 13.735 s; *Car8*^{wdl} treated = 68.411 ± 11.915 s; p = 1.281×10^{-146}; Fig. 6O). These data show that while CHZ corrects most properties of Purkinje cell firing, it only partially rescues motor behavior in

Car8^{wdl} mice. This finding prompted us to ask whether the *Car8*^{wdl} mutant phenotype might involve developmental/circuit connectivity abnormalities that are resistant to the particular type of benefits that CHZ can provide for recovery.

Purkinje cell firing is already compromised in pre-weaned developing pups

If there are early wiring problems in *Car8*^{wdl}, then even corrected signals might be corrupted because they still have to travel through a miswired circuit. In P18 and P21 control mice, Purkinje cells fire more slowly and with decreased regularity compared to adult mice (Arancillo et al., 2015; Fig. 8). *Car8*^{wdl} Purkinje cells of the same ages fire more rapidly (control SS frequency = 22.405 ± 2.928 Hz; *Car8*^{wdl} SS frequency = 38.681 ± 5.338 Hz; p = 0.015; Fig. 8) and with even less regularity than young control cells (control SS CV = 2.674 ± 0.255; *Car8*^{wdl} SS CV = 4.25 ± 1.14; p = 0.126; Fig. 8), although not significantly. Purkinje cells in young *Car8*^{wdl} mice do fire with decreased CV2, suggesting that, similar to the adult characteristic, local firing is more regular (control SS CV2 = 0.428 ± 0.041; *Car8*^{wdl} SS CV2 = 0.241 ± 0.024; p = 9.86×10^{-5}; Fig. 8). In fact, the Purkinje cells of young *Car8*^{wdl} mice fire at a frequency similar to adult control and *Car8*^{wdl} mice (Fig. 8). Additionally, Purkinje cells of *Car8*^{wdl} mice have a similar % of pauses in SS over 100 ms to adults (young *Car8*^{wdl} SS % over 100 ms = 0.903 ± 0.345; adult *Car8*^{wdl} SS % over 100 ms = 0.566 ± 0.179; p = 0.395; Fig. 8). Because of the firing pattern of young Purkinje cells in control mice, young *Car8*^{wdl} Purkinje cells have a lower % of pauses over 100 ms (young control SS % over 100 ms = 6.466 ± 2.362; young *Car8*^{wdl} SS % over 100 ms = 0.903 ± 0.345; p = 0.039; Fig. 8). In adult animals, after control Purkinje cells have normalized in their pattern of firing, *Car8*^{wdl} Purkinje cells have a much higher % of pauses over 100 ms (adult control SS % over 100 ms = 0.0828 ± 0.066; adult *Car8*^{wdl} SS % over 100 ms = 0.566 ± 0.179; p = 0.0197; Fig. 8). Although weanling Purkinje cells tend to have a decreased CS rate, young *Car8*^{wdl} Purkinje cells fire an even lower CS rate compared to controls (control CS frequency = 0.571 ± 0.072; *Car8*^{wdl} CS frequency = 0.225 ± 0.047; p = 7.31×10^{-4}; Fig. 8). CS CV is unchanged between young *Car8*^{wdl} Purkinje cells and young controls (control CS CV = 0.625 ± 0.014; *Car8*^{wdl} CS CV = 0.725 ± 0.049; p = 0.070; Fig. 8). However, CS CV2 is significantly higher in young *Car8*^{wdl} Purkinje cells (weanling control CS CV2 = 0.757 ± 0.014; weanling *Car8*^{wdl} CS CV2 = 0.847 ± 0.031; p = 0.0145; Fig. 8). This is in contrast to the adults where *Car8*^{wdl} CS CV2 is lower than controls (Fig. 6). This is likely due to the increase in CS CV2 of control Purkinje cells from weanling age to adulthood (weanling CS CV2 = 0.757 ± 0.014; adult CS CV2 = 0.953 ± 0.034; p = 9.109×10^{-5}), whereas *Car8*^{wdl} CS CV2 shows a slight but significant decrease with age (weanling CS CV2 = 0.847 ± 0.031; adult CS CV2 = 0.750 ± 0.027; p = 0.0259). These data suggest that cerebellar circuitry is dysfunctional early in *Car8*^{wdl}, and although there is a recovery of cerebellar cortical thickness during development (Fig. 3), the functions of the microcircuits contained within the cortex remain defective. Indeed, previous work demonstrated that cerebellar morphogenesis and circuit wiring are independently controlled (Sillitoe et al., 2010). We postulate that the early structural (Fig. 5, Fig. S4) and functional (Fig. 8) connectivity problems in *Car8*^{wdl} may hinder the beneficial effects of CHZ.

CHZ does not reconfigure the miswired cerebellar circuit map in *Car8^{wdl}* mice

To examine whether CHZ corrects circuit miswiring, we treated P30-P60 mice with CHZ for 10 days and then examined the expression of zebrinII and PLCβ4 as a readout for wiring (n = 4). CHZ treatment did not have any effect on the zonal map since zebrinII and PLCβ4 still had overlapping domains with poorly defined boundaries (Fig. S5). These data led us to ask whether there are persistent defects in the zonal plan that we could use to link circuit patterning, in a more dynamic way, to the progressive nature of the ataxia and the tremor. To assess this, we looked to see if tyrosine hydroxylase (TH) was ectopically expressed in *Car8^{wdl}* Purkinje cells.

Dynamic TH expression reflects progressive changes in Purkinje cell zones of *Car8^{wdl}*

TH is a precursor for dopamine, norepinephrine and epinephrine (Daubner et al., 2011). In ataxic mice, TH is ectopically up-regulated in Purkinje cells (Sawada and Fukui, 2001); its presence is thought to result from Ca^{2+} dysregulation (Sawada and Fukui, 2001). Because CAR8 interacts with IP3R1 (Hirota et al., 2003), we predicted that the loss of *Car8* might induce ectopic TH expression. At P30, we found low TH levels in the vermis of control and *Car8^{wdl}* mice (Fig. 9; n = 3 each). TH expression increases in intensity and spreads to more lobules as *Car8^{wdl}* mice age, (Fig. 9, Fig. S6; n = 3 mice of each genotype and age). *TH* mRNA also increases as *Car8^{wdl}* mice age (Fig. S7). We found the most intense and widespread distribution of *TH* in P300 *Car8^{wdl}* mice compared to P20 mutants, P20 controls, and P300 controls (Fig. S7). Interestingly, the ectopic TH protein and mRNA were expressed in a zonal pattern (Fig. 9, Fig. S7). Thus, despite the recovery of the zebrinII-HSP25 relationship, TH expression points to persistent molecular defects within the zonal architecture. Next, we sought to determine the cellular mechanism that controls ectopic TH, and whether targeting this mechanism could lower TH to the control levels.

Ca^{2+} channels mediate ectopic tyrosine hydroxylase expression in *Car8^{wdl}* Purkinje cells

A single dose of nimodipine, which blocks voltage-gated calcium channels (Stengel et al., 1998, Zheng and Raman, 2011), lowers TH expression in ataxic *tottering* mice to control levels (Fureman et al., 1999). The *tottering* mouse has a mutation in the alpha1A subunit of the $Ca_V2.1$ (P/Q type) voltage-gated Ca^{2+} channel (Fletcher et al., 1996). A single dose of nimodipine also lowered TH in *Car8^{wdl}* (Fig. 9K; n = 4) whereas CHZ failed to decrease it (Fig. 9L; n = 3). These data suggest that the ectopic TH is Ca^{2+} mediated, and in *Car8^{wdl}*, the progressive TH response may reflect sustained Ca^{2+} defects. Drugs that control Ca^{2+} homeostasis may therefore be good therapeutic options. Support for this idea was shown in a mouse model of SCA28 (Maltecca et al., 2015).

DISCUSSION

There is a major emphasis on understanding the mechanisms of neurodegeneration because of the impact that it has on brain function and behavior. Such studies have far reaching implications because of the prospect of identifying common themes across diseases. We focused on how motor diseases destroy movement and learning, but instead, in the absence of neurodegeneration.

Mutations in *CA8*, *VLDLR*, *WDR81*, and *ATP8A2* belong to a class of heterogeneous but related conditions that are classified by ataxia, disequilibrium, and in some cases mental retardation (Ali et al., 2012). Genetic studies in mice and zebrafish show that loss of these genes mimics the main behavioral features of the human condition, and in each case Purkinje cells are the primary target (Jiao et al., 2005, Trommsdorff et al., 1999, Traka et al., 2013, Aspatwar et al., 2012). And, although Purkinje cell degeneration is a recurring feature of motor disease, it is intriguing that behavior can be affected early in life and without obvious structural pathology in the cerebellum (White et al., 2014). This raises important questions about the mechanisms for how Purkinje cells impact movement. By focusing our attention on *Car8* function, we revealed their roles during circuit formation, circuit function, and the deterioration of motor behavior with age.

The most unexpected finding that we made was the lack of Purkinje cell degeneration in aging *Car8*^{wdl} mice, despite the progressive worsening of motor function, motor learning, and tremor. To understand how this might occur, we turned our attention to the fundamental organization of the cerebellum into zones. Zones are central to cerebellar development, function, behavior, and even disease (Cerminara et al., 2015) and improper targeting of cerebellar circuitry leads to severe motor defects (Armstrong et al., 2009, Croci et al., 2006, Sillitoe et al., 2010, Badura et al., 2013). We found that loss of CAR8 severely affected the spatial and temporal development of Purkinje cell zones, and as a consequence sensory maps failed to acquire their unique positional information. This phenotype is very similar to what is observed when the $Ca_V2.1$ Ca^{2+} channel is removed from Purkinje cells (Miyazaki et al., 2012), which is interesting because CAR8 may influence Ca^{2+} regulation. Our data revealed that Ca^{2+} might have a long-lasting impact on zones in *Car8*^{wdl}. We found a dramatic increase in ectopic TH in Purkinje cell zones, and with age the intensity increased. Blocking Ca^{2+} influx into Purkinje cells lowered TH, but treating the mice with CHZ, the Ca^{2+}-dependent K^+ channel agonist that corrects abnormal Purkinje cell activity, had no effect on TH (see below). These surprising results have broad implications for brain disease because it stimulates the idea that beyond the “visible” pathologies such as Tau and tangle accumulation or dendrite retraction, a more cryptic and dynamic molecular neuropathology might exist in many conditions. Therefore, it may be important to consider the possibility of using precise molecular readouts, such as patterned TH expression, as potential biomarkers for disease progression. Collectively however, our data argue that loss of *Car8* disrupted the functional platform upon which cerebellar circuitry is built and maintained, which led us to ask if, and to what extent, neural activity was altered in the preserved circuits.

Indeed, we found using an *in vivo* recording approach that excitatory CS activity is significantly reduced in *Car8*^{wdl} Purkinje cells (Fig. 6). But, it was the irregular pattern of high frequency SS firing with long pauses interrupting the spike train that was of specific interest to disease related behavior. Cerebellar neurons exhibit very irregular firing patterns in rodent models of ataxia (Gao et al., 2012), dystonia (LeDoux, 2011), and even multiple sclerosis (Saab et al., 2004). This irregular and sometimes erratic firing may be a major factor contributing to the abnormal motor behavior (Alvina and Khodakhah, 2010, Fremont et al., 2014), although it is still unclear how this mode of firing influences motor defects (Stahl and Thumser, 2014), especially in the absence of cell loss. We tested this possibility

by feeding CHZ to *Car8*^{wdl} adults using a paradigm that has previously been used to correct Purkinje cell firing (Alvina and Khodakhah, 2010; Gao et al., 2012). We found that CHZ corrects some properties of Purkinje cell firing. But, although motor performance on the rotarod improved significantly, we failed to recover it to control levels (Fig. 6). We also failed to repair the zebrinII zone defects with CHZ, indicating that circuit mispatterning plus circuit dysfunction contribute to the motor deficits in *Car8*^{wdl}. These deficits may arise from developmental alterations that promote periods of high frequency firing with local changes in spike regularity. Ultimately, the abnormal motor behaviors in *Car8*^{wdl} are likely mediated by altered cerebellar nuclear output (Hoebeek et al., 2008, Fremont et al., 2014). The misfiring of Purkinje cell CS's in *Car8*^{wdl} implies that defective cerebellar nuclear output results in a decrease in inferior olive feedback to the cerebellum (Chaumont et al., 2013, Witter et al., 2013, White et al., 2014), pointing to circuit loop defects that may be operating within the modules. But, our data do not exclude the possibility that the motor dysfunction in *Car8*^{wdl} mice may be due to altered parallel fiber to Purkinje cell connectivity (Hirasawa et al., 2007). However, this particular defect may be more critical for the learning abnormalities with a limited impact on ongoing movement (Fig. 2; Galliano et al., 2013). We therefore conclude that *Car8* gene function impacts behavior, at least in part, by patterning the cerebellum into functional circuits that mediate ataxia and tremor. This is particularly interesting because recent work shows that human essential tremor may involve wiring changes in the Purkinje cell microcircuit (Louis, 2014). Our current study thus lays the foundation to further investigate the mechanisms of how brain diseases impact behavior when there are no typical signs of neurodegeneration.

In addition to the ectopic TH expression, the mis-patterning of cerebellar afferent domains may represent an atypical mode of neurodegeneration. But, how could defects in the circuit projection map potentially contribute to the motor dysfunction in *Car8*^{wdl}? Ataxia, dystonia, and tremor all interfere with normal muscle control. To execute smooth movements, the muscles must cooperate in a process that requires agonist and antagonist muscles to work together, rather than against one another. For example, during elbow flexion, contraction of the biceps is accompanied by relaxation of the triceps. Loss of this process could be at core of ataxia and dystonia, since both diseases exhibit forms of prolongation of agonist activity and mistimed antagonist activity (Shakkottai, 2014). Given the ataxia and dystonia observed in *Car8*^{wdl} (Jiao et al., 2005), our data showing the convergence of VGLUT2-expressing spinocerebellar and VGLUT1-expressing cuneocerebellar projection zones might provide the anatomical substrate for the muscle incoordination (Fig. 5E). In accordance with this, transynaptic tracing from the muscles back to the cerebellar cortex suggest that individual Purkinje cell zones may control synergistic muscle activity (Ruigrok et al., 2008). In the *Car8*^{wdl} model, loss of muscle synergy might stem from a miswiring of the functional circuit map after loss of CAR8 in Purkinje cells (Fig. 5D). Specifically, the patterning of map is affected in early postnatal *Car8*^{wdl} mice, although it is possible that multiple stages of afferent ingrowth are affected (Arsenio Nunes and Sotelo, 1985). It is interesting to speculate that the zonal segregation of sensory-motor circuits directly facilitates Purkinje cell computations that instruct the temporal activation of agonist and antagonist muscle groups for precise motor responses. Taken together, our data broaden the impact of

neurodegeneration on cerebellar function to include developmental wiring problems that, over time, instigate multiple circuit defects that culminate into poor control of the muscles.

CONCLUSIONS

Neurodegeneration influences the outcome of motor and non-motor neurological diseases. In this study, we used the cerebellum as a model to test how disease onset and progression impact behavior when there is no neurodegeneration. We found that defective circuit patterning leads to alterations in circuit wiring and changes in neural activity, which ultimately caused ataxia and tremor. Motor behavior could be rescued by restoring neuronal function. These findings unveil the developmental origins of brain diseases that progress without typical signs of degeneration.

Supplementary Material

Refer to Web version on PubMed Central for supplementary material.

ACKNOWLEDGEMENTS

This work was supported by the Bachmann-Strauss Dystonia and Parkinson Foundation Inc. (R.V.S.), BCM IDDRC Grant U54HD083092 (R.V.S.), NINDS R01 NS089664 (R.V.S.) and F31 NS092264 (J.J.W.). The BCM IDDRC Neuropathology Core performed the tissue staining and histopathology experiments. The behavior experiments were conducted in the BCM IDDRC Mouse Neurobehavioral Core. The content is solely the responsibility of the authors and does not necessarily represent the official views of the NIH. M.A. received support from the National Ataxia Foundation (NAF). The initial anatomical and expression experiments were conducted at Albert Einstein College of Medicine (S.A.G. and R.V.S.).

REFERENCES

Ali BR, Silhavy JL, Gleeson MJ, Gleeson JG, Al-Gazali L. A missense founder mutation in *VLDLR* is associated with Dysequilibrium Syndrome without quadrupedal locomotion. BMC Medical Genetics. 2012; 13

Alvina K, Khodakhah K. KCa channels as therapeutic targets in episodic ataxia type-2. J Neurosci. 2010; 30:7249–7257. [PubMed: 20505091]

Apps R, Hawkes R. Cerebellar cortical organization: a one-map hypothesis. Nature reviews Neuroscience. 2009; 10:670–681. [PubMed: 19693030]

Arancillo M, White JJ, Lin T, Stay TL, Sillitoe RV. In vivo analysis of Purkinje cell firing properties during postnatal mouse development. J Neurophysiol. 2015; 113:578–591. [PubMed: 25355961]

Armstrong CL, Chung SH, Armstrong JN, Hochgeschwender U, Jeong YG, Hawkes R. A novel somatostatin-immunoreactive mossy fiber pathway associated with HSP25-immunoreactive purkinje cell stripes in the mouse cerebellum. J Comp Neurol. 2009; 517:524–538. [PubMed: 19795496]

Armstrong CL, Hawkes R. Pattern formation in the cerebellar cortex. Biochem Cell Biol. 2000; 78:551–562. [PubMed: 11103945]

Armstrong CL, Krueger-Naug AM, Currie RW, Hawkes R. Constitutive expression of the 25-kDa heat shock protein Hsp25 reveals novel parasagittal bands of purkinje cells in the adult mouse cerebellar cortex. J Comp Neurol. 2000; 416:383–397. [PubMed: 10602096]

Arsenio Nunes ML, Sotelo C. Development of the spinocerebellar system in the postnatal rat. J Comp Neurol. 1985; 237:291–306. [PubMed: 3840179]

Aspatwar A, Tolvanen ME, Jokitalo E, Parikka M, Ortutay C, Harjula SK, Ramet M, Vihinen M, Parkkila S. Abnormal cerebellar development and ataxia in CARP VIII morphant zebrafish. Hum Mol Genet. 2012; 22:417–432. [PubMed: 23087022]

Badura A, Schonewille M, Voges K, Galliano E, Renier N, Gao Z, Witter L, Hoebeek FE, Chedotal A, De Zeeuw CI. Climbing fiber input shapes reciprocity of Purkinje cell firing. Neuron. 2013; 78:700–713. [PubMed: 23643935]

Bosco G, Poppele RE. Proprioception from a spinocerebellar perspective. Physiol Rev. 2001; 81:539–568. [PubMed: 11274339]

Brochu G, Maler L, Hawkes R. Zebrin II: a polypeptide antigen expressed selectively by Purkinje cells reveals compartments in rat and fish cerebellum. J Comp Neurol. 1990; 291:538–552. [PubMed: 2329190]

Cerminara NL, Lang EJ, Sillitoe RV, Apps R. Redefining the cerebellar cortex as an assembly of non-uniform Purkinje cell microcircuits. Nature reviews Neuroscience. 2015; 16:79–93. [PubMed: 25601779]

Chaumont J, Guyon N, Valera AM, Dugue GP, Popa D, Marcaggi P, Gautheron V, Reibel-Foisset S, Dieudonne S, Stephan A, et al. Clusters of cerebellar Purkinje cells control their afferent climbing fiber discharge. Proc Natl Acad Sci U S A. 2013; 110:16223–16228. [PubMed: 24046366]

Chen X, Kovalchuk Y, Adelsberger H, Henning HA, Sausbier M, Wietzorrek G, Ruth P, Yarom Y, Konnerth A. Disruption of the olivo-cerebellar circuit by Purkinje neuron-specific ablation of BK channels. Proc Natl Acad Sci U S A. 2010; 107:12323–12328. [PubMed: 20566869]

Croci L, Chung SH, Masserdotti G, Gianola S, Bizzoca A, Gennarini G, Corradi A, Rossi F, Hawkes R, Consalez GG. A key role for the HLH transcription factor EBF2COE2,O/E-3 in Purkinje neuron migration and cerebellar cortical topography. Development. 2006; 133:2719–2729. [PubMed: 16774995]

Daubner SC, Le T, Wang S. Tyrosine hydroxylase and regulation of dopamine synthesis. Arch Biochem Biophys. 2011; 508:1–12. [PubMed: 21176768]

Elble RJ. Essential tremor frequency decreases with time. Neurology. 2000; 55:1547–1551. [PubMed: 11094112]

Fletcher CF, Lutz CM, O'Sullivan T, Shaughnessy J. Absence epilepsy in tottering mutant mice is associated with calcium channel defects. Cell. 1996

Fremont R, Calderon DP, Maleki S, Khodakhah K. Abnormal high-frequency burst firing of cerebellar neurons in rapid-onset dystonia-parkinsonism. J Neurosci. 2014; 34:11723–11732. [PubMed: 25164667]

Fu Y, Tvrdik P, Makki N, Paxinos G, Watson C. Precerebellar cell groups in the hindbrain of the mouse defined by retrograde tracing and correlated with cumulative Wnt1-cre genetic labeling. Cerebellum. 2011; 10:570–584. [PubMed: 21479970]

Fureman BE, Campbell DB, Hess EJ. L-type calcium channel regulation of abnormal tyrosine hydroxylase expression in cerebella of tottering mice. Ann N Y Acad Sci. 1999; 868:217–219. [PubMed: 10414297]

Galliano E, Potters JW, Elgersma Y, Wisden W, Kushner SA, De Zeeuw CI, Hoebeek FE. Synaptic transmission and plasticity at inputs to murine cerebellar Purkinje cells are largely dispensable for standard nonmotor tasks. J Neurosci. 2013; 33:12599–12618. [PubMed: 23904597]

Gao Z, Todorov B, Barrett CF, van Dorp S, Ferrari MD, van den Maagdenberg AM, De Zeeuw CI, Hoebeek FE. Cerebellar ataxia by enhanced Ca(V)2.1 currents is alleviated by Ca2+-dependent K+-channel activators in Cacna1a(S218L) mutant mice. J Neurosci. 2012; 32:15533–15546. [PubMed: 23115190]

Gebre SA, Reeber SL, Sillitoe RV. Parasagittal compartmentation of cerebellar mossy fibers as revealed by the patterned expression of vesicular glutamate transporters VGLUT1 and VGLUT2. Brain Struct Funct. 2012; 217:165–180. [PubMed: 21814870]

Gennarino VA, Singh RK, White JJ, De Maio A, Han K, Kim JY, Jafar-Nejad P, di Ronza A, Kang H, Sayegh LS, et al. Pumilio1 Haploinsufficiency Leads to SCA1-like Neurodegeneration by Increasing Wild-Type Ataxin1 Levels. Cell. 2015; 160:1087–1098. [PubMed: 25768905]

Handforth A. Harmaline tremor: underlying mechanisms in a potential animal model of essential tremor. Tremor Other Hyperkinet Mov (NY). 2012; 2

Hirasawa M, Xu X, Trask RB, Maddatu TP, Johnson BA, Naggert JK, Nishina PM, Ikeda A. Carbonic anhydrase related protein 8 mutation results in aberrant synaptic morphology and excitatory synaptic function in the cerebellum. Mol Cell Neurosci. 2007; 35:161–170. [PubMed: 17376701]

Hirota J, Ando H, Hamada K, Mikoshiba K. Carbonic anhydrase-related protein is a novel binding protein for inositol 1,4,5-trisphosphate receptor type 1. Biochem J. 2003; 372:435–441. [PubMed: 12611586]

Hoebeek FE, Khosrovani S, Witter L, De Zeeuw CI. Purkinje cell input to cerebellar nuclei in tottering: ultrastructure and physiology. Cerebellum. 2008; 7:547–558. [PubMed: 19082682]

Jiao Y, Yan J, Zhao Y, Donahue LR, Beamer WG, Li X, Roe BA, Ledoux MS, Gu W. Carbonic anhydrase-related protein VIII deficiency is associated with a distinctive lifelong gait disorder in waddles mice. Genetics. 2005; 171:1239–1246. [PubMed: 16118194]

Kato K. Sequence of a novel carbonic anhydrase-related polypeptide and its exclusive presence in Purkinje cells. FEBS Lett. 1990; 271:137–140. [PubMed: 2121526]

Lakkis MM, Bergenhem NC, O'Shea KS, Tashian RE. Expression of the acatalytic carbonic anhydrase VIII gene, Car8, during mouse embryonic development. Histochem J. 1997a; 29:135–141. [PubMed: 9147070]

Lakkis MM, O'Shea KS, Tashian RE. Differential expression of the carbonic anhydrase genes for CA VII (Car7) and CA-RP VIII (Car8) in mouse brain. J Histochem Cytochem. 1997b; 45:657–662. [PubMed: 9154152]

Larsell, O. The Comparative Anatomy and Histology of the Cerebellum From Monotremes Through Apes. Minneapolis: University of Minnesota Press; 1970.

LeDoux MS. Animal models of dystonia: Lessons from a mutant rat. Neurobiol Dis. 2011; 42:152–161. [PubMed: 21081162]

Louis ED. Re-thinking the biology of essential tremor: From models to morphology. Parkinsonism & related disorders. 2014; 20:S88–S93. [PubMed: 24262197]

Louis ED, Faust PL, Vonsattel JP. Purkinje cell loss is a characteristic of essential tremor. Parkinsonism & related disorders. 2011; 17:406–409. [PubMed: 21600832]

Maltecca F, Baseggio E, Consolato F, Mazza D, Podini P, Young SM Jr, Drago I, Bahr BA, Puliti A, Codazzi F, et al. Purkinje neuron Ca2+ influx reduction rescues ataxia in SCA28 model. J Clin Invest. 2015; 125:263–274. [PubMed: 25485680]

Miwa H. Rodent models of tremor. Cerebellum. 2007; 6:66–72. [PubMed: 17366267]

Miyazaki T, Yamasaki M, Hashimoto K, Yamazaki M, Abe M, Usui H, Kano M, Sakimura K, Watanabe M. Cav2.1 in cerebellar Purkinje cells regulates competitive excitatory synaptic wiring, cell survival, and cerebellar biochemical compartmentalization. J Neurosci. 2012; 32:1311–1328. [PubMed: 22279216]

Orr HT. Cell biology of spinocerebellar ataxia. J Cell Biol. 2012; 197:167–177. [PubMed: 22508507]

Pandolfo M. Friedreich ataxia. Arch Neurol. 2008; 65:1296–1303. [PubMed: 18852343]

Park YG, Park HY, Lee CJ, Choi S, Jo S, Choi H, Kim YH, Shin HS, Llinas RR, Kim D. Ca(V)3.1 is a tremor rhythm pacemaker in the inferior olive. Proc Natl Acad Sci U S A. 2010; 107:10731–10736. [PubMed: 20498062]

Prudente CN, Pardo CA, Xiao J, Hanfelt J, Hess EJ, Ledoux MS, Jinnah HA. Neuropathology of cervical dystonia. Exp Neurol. 2013; 241:95–104. [PubMed: 23195594]

Ruigrok TJ, Pijpers A, Goedknegt-Sabel E, Coulon P. Multiple cerebellar zones are involved in the control of individual muscles: a retrograde transneuronal tracing study with rabies virus in the rat. Eur J Neurosci. 2008; 28:181–200. [PubMed: 18662342]

Saab CY, Craner MJ, Kataoka Y, Waxman SG. Abnormal Purkinje cell activity in vivo in experimental allergic encephalomyelitis. Exp Brain Res. 2004; 158:1–8. [PubMed: 15118796]

Sarna JR, Hawkes R. Patterned Purkinje cell death in the cerebellum. Prog Neurobiol. 2003; 70:473–507. [PubMed: 14568361]

Sarna JR, Larouche M, Marzban H, Sillitoe RV, Rancourt DE, Hawkes R. Patterned Purkinje cell degeneration in mouse models of Niemann-Pick type C disease. J Comp Neurol. 2003; 456:279–291. [PubMed: 12528192]

Sarna JR, Marzban H, Watanabe M, Hawkes R. Complementary stripes of phospholipase Cbeta3 and Cbeta4 expression by Purkinje cell subsets in the mouse cerebellum. J Comp Neurol. 2006; 496:303–313. [PubMed: 16566000]

Sawada K, Fukui Y. Expression of tyrosine hydroxylase in cerebellar Purkinje cells of ataxic mutant mice: its relation to the onset and/or development of ataxia. J Med Invest. 2001; 48:5–10. [PubMed: 11286017]

Shakkottai VG. Physiologic changes associated with cerebellar dystonia. Cerebellum. 2014; 13:637–644. [PubMed: 24879387]

Shakkottai VG, do Carmo Costa M, Dell'Orco JM, Sankaranarayanan A, Wulff H, Paulson HL. Early changes in cerebellar physiology accompany motor dysfunction in the polyglutamine disease spinocerebellar ataxia type 3. J Neurosci. 2011; 31:13002–13014. [PubMed: 21900579]

Sillitoe RV, Benson MA, Blake DJ, Hawkes R. Abnormal dysbindin expression in cerebellar mossy fiber synapses in the mdx mouse model of Duchenne muscular dystrophy. J Neurosci. 2003; 23:6576–6585. [PubMed: 12878699]

Sillitoe RV, Vogel MW, Joyner AL. Engrailed homeobox genes regulate establishment of the cerebellar afferent circuit map. J Neurosci. 2010; 30:10015–10024. [PubMed: 20668186]

Sotelo C. Cellular and genetic regulation of the development of the cerebellar system. Prog Neurobiol. 2004; 72:295–339. [PubMed: 15157725]

Stahl JS, Thumser ZC. Flocculus Purkinje cell signals in mouse Cacna1a calcium channel mutants of escalating severity: an investigation of the role of firing irregularity in ataxia. J Neurophysiol. 2014; 112:2647–2663. [PubMed: 25143538]

Stengel W, Jainz M, Andreas K. Different potencies of dihydropyridine derivatives in blocking T-type but not L-type Ca 2+ channels in neuroblastoma-glioma hybrid cells. Eur J Pharmacol. 1998; 342:339–345. [PubMed: 9548406]

Taniuchi K, Nishimori I, Takeuchi T, Fujikawa-Adachi K, Ohtsuki Y, Onishi S. Developmental expression of carbonic anhydrase-related proteins VIII, X, and XI in the human brain. Neuroscience. 2002; 112:93–99. [PubMed: 12044474]

Thanvi B, Lo N, Robinson T. Essential tremor-the most common movement disorder in older people. Age Ageing. 2006; 35:344–349. [PubMed: 16641144]

Traka M, Millen KJ, Collins D, Elbaz B, Kidd GJ, Gomez CM, Popko B. WDR81 is necessary for purkinje and photoreceptor cell survival. J Neurosci. 2013; 33:6834–6844. [PubMed: 23595742]

Tripp BC, Smith K, Ferry JG. Carbonic anhydrase: new insights for an ancient enzyme. J Biol Chem. 2001; 276:48615–48618. [PubMed: 11696553]

Trommsdorff M, Gotthardt M, Hiesberger T, Shelton J, Stockinger W, Nimpf J, Hammer RE, Richardson JA, Herz J. Reeler/Disabled-like disruption of neuronal migration in knockout mice lacking the VLDL receptor and ApoE receptor 2. Cell. 1999; 97:689–701. [PubMed: 10380922]

Turkmen S, Guo G, Garshasbi M, Hoffmann K, Alshalah AJ, Mischung C, Kuss A, Humphrey N, Mundlos S, Robinson PN. CA8 mutations cause a novel syndrome characterized by ataxia and mild mental retardation with predisposition to quadrupedal gait. PLoS Genet. 2009; 5:e1000487. [PubMed: 19461874]

Unno T, Wakamori M, Koike M, Uchiyama Y, Ishikawa K, Kubota H, Yoshida T, Sasakawa H, Peters C, Mizusawa H, et al. Development of Purkinje cell degeneration in a knockin mouse model reveals lysosomal involvement in the pathogenesis of SCA6. Proc Natl Acad Sci U S A. 2012; 109:17693–17698. [PubMed: 23054835]

Van de Leemput J, Chandran J, Knight M, Holtzclaw L, Scholz S, Cookson MR, Houlden H, Gwinn K, Fung P, Lin X, et al. Deletion at ITPR1 underlies ataxia in mice and humans (SCA15). PLoS Genetics. 2007:e108. *preprint*. [PubMed: 17590087]

Welsh JP, Yuen G, Placantonakis DG, Vu TQ, Haiss F, O'hearn E, Molliver M, Aicher SA. Why do Purkinje cells die so easily after global brain ischemia? Aldolase C, EAAT4, and the cerebellar contribution to posthypoxic myoclonus. Adv Neurol. 2002; 89:331–359. [PubMed: 11968459]

White JJ, Arancillo M, Stay T, George-Jones NA, Levy SL, Heck DH, Sillitoe RV. Cerebellar Zonal Patterning Relies on Purkinje Cell Neurotransmission. J Neurosci. 2014; 34:8231–8245. [PubMed: 24920627]

White JJ, Sillitoe RV. Postnatal development of cerebellar zones revealed by neurofilament heavy chain protein expression. Front Neuroanat. 2013; 7:9. [PubMed: 23675325]

Williams BL, Yaddanapudi K, Hornig M, Lipkin WI. Spatiotemporal analysis of purkinje cell degeneration relative to parasagittal expression domains in a model of neonatal viral infection. J Virol. 2007; 81:2675–2687. [PubMed: 17182680]

Wilson BK, Hess EJ. Animal models for dystonia. Mov Disord. 2013; 28:982–989. [PubMed: 23893454]

Witter L, Canto CB, Hoogland TM, de Gruijl JR, De Zeeuw CI. Strength and timing of motor responses mediated by rebound firing in the cerebellar nuclei after Purkinje cell activation. Frontiers in neural circuits. 2013; 7:133. [PubMed: 23970855]

Zheng N, Raman IM. Prolonged postinhibitory rebound firing in the cerebellar nuclei mediated by group I metabotropic glutamate receptor potentiation of L-type calcium currents. J Neurosci. 2011; 31:10283–10292. [PubMed: 21753005]

HIGHLIGHTS

- *Car8*^{wdl} mice exhibit ataxia and key physiological features of essential tremor
- Motor dysfunction in *Car8*^{wdl} mice progresses without typical signs of degeneration
- Circuit wiring and neuronal activity determine the *Car8*^{wdl} mutant phenotype
- Cerebellar zone defects may reflect a cryptic code for neurological decline with age

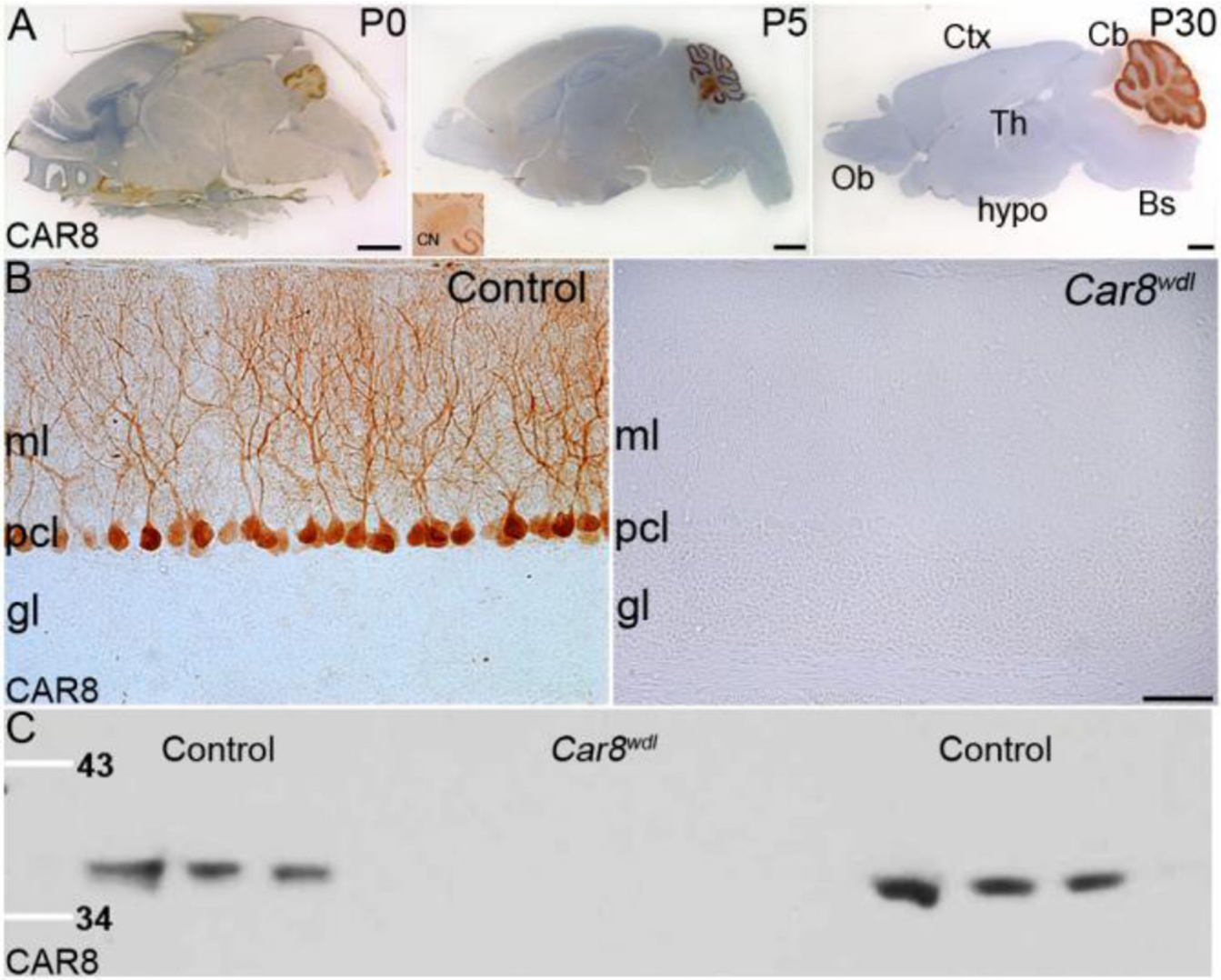

Figure 1. CAR8 is heavily expressed in control Purkinje cells and is absent in *Car8^{wdl}*

CAR8 protein is heavily expressed in early postnatal (P0 and P5) and adult Purkinje cells (P30 shown) (A). Inset in the middle panel shows CAR8 immunopositive Purkinje cell terminals in the cerebellar nuclei (CN). Note that the cerebellar nuclear neurons themselves do not express CAR8 (White et al., 2014). Scale bars = 500 μm. Abbreviations: ml = molecular layer, pcl = Purkinje cell layer, gl = granular layer, CN = cerebellar nuclei. CAR8 protein is expressed in the soma and dendrites of control Purkinje cells but is absent from Purkinje cells in *Car8^{wdl}* (B). Scale bar = 50 μm. CAR8 protein is not detected in lysates from *Car8^{wdl}* cerebellar tissue (C). 6 controls and 3 mutants are shown.

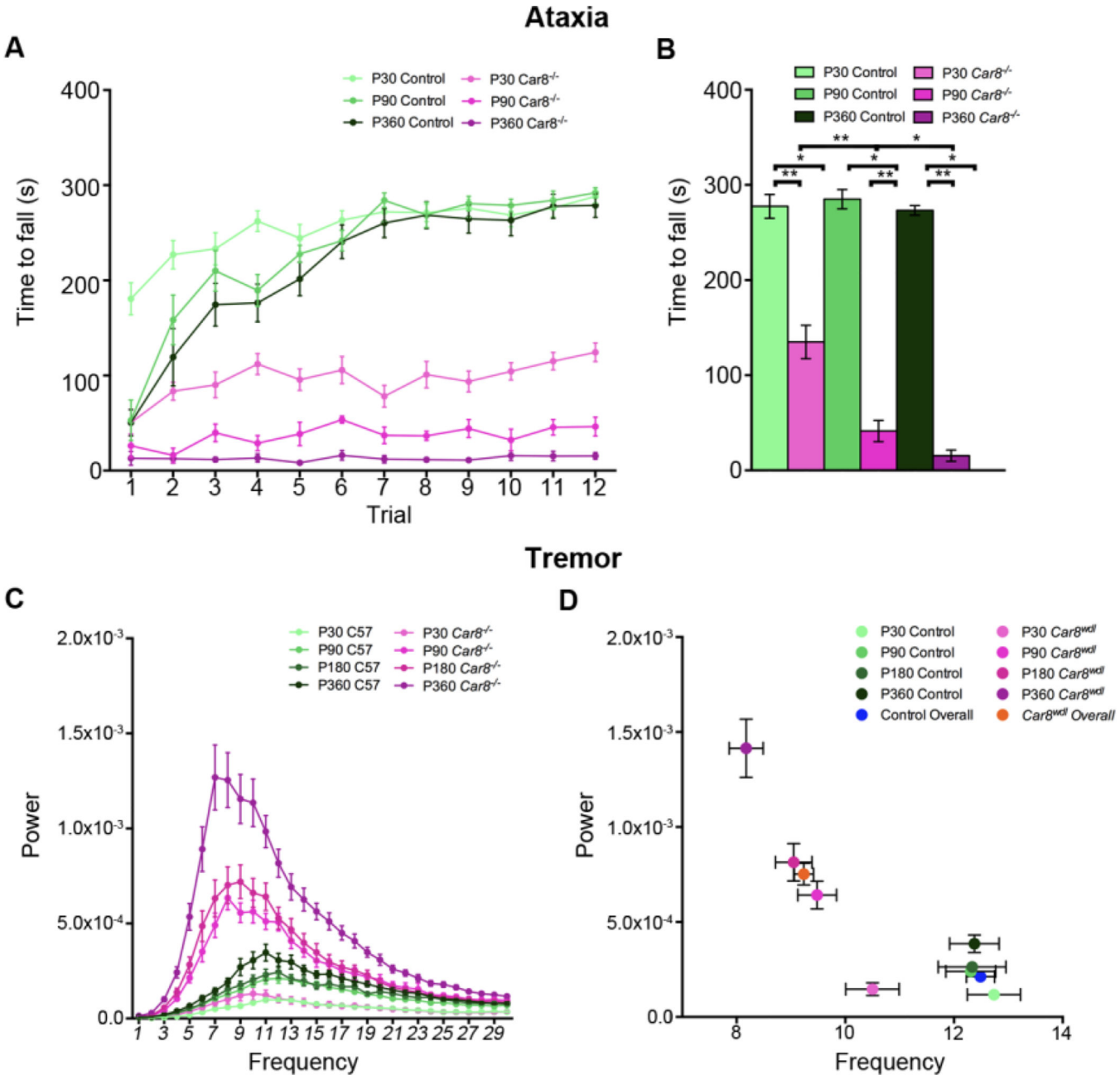

Figure 2. *Car8*^{wdl} mice have motor abnormalities that intensify with age

Training over four days on the accelerating rotarod reveals deficits in motor performance in *Car8*^{wdl} mice. This deficit becomes more pronounced as the mutant mice age (A). Analysis of the last day of training reveals no significant difference between control mice across different ages (B). *Car8*^{wdl} mice perform significantly worse than their age matched controls at each age. Additionally, older *Car8*^{wdl} mice perform significantly worse than younger *Car8*^{wdl} mice. *Car8*^{wdl} mice display a pronounced tremor as compared to control mice. The amplitude (power) of tremor in *Car8*^{wdl} mice becomes more pronounced with age (C). *Car8*^{wdl} mice display a tremor that increases in amplitude but decreases in frequency with

age (D). Control physiological tremor also increases with age but does not change in frequency.

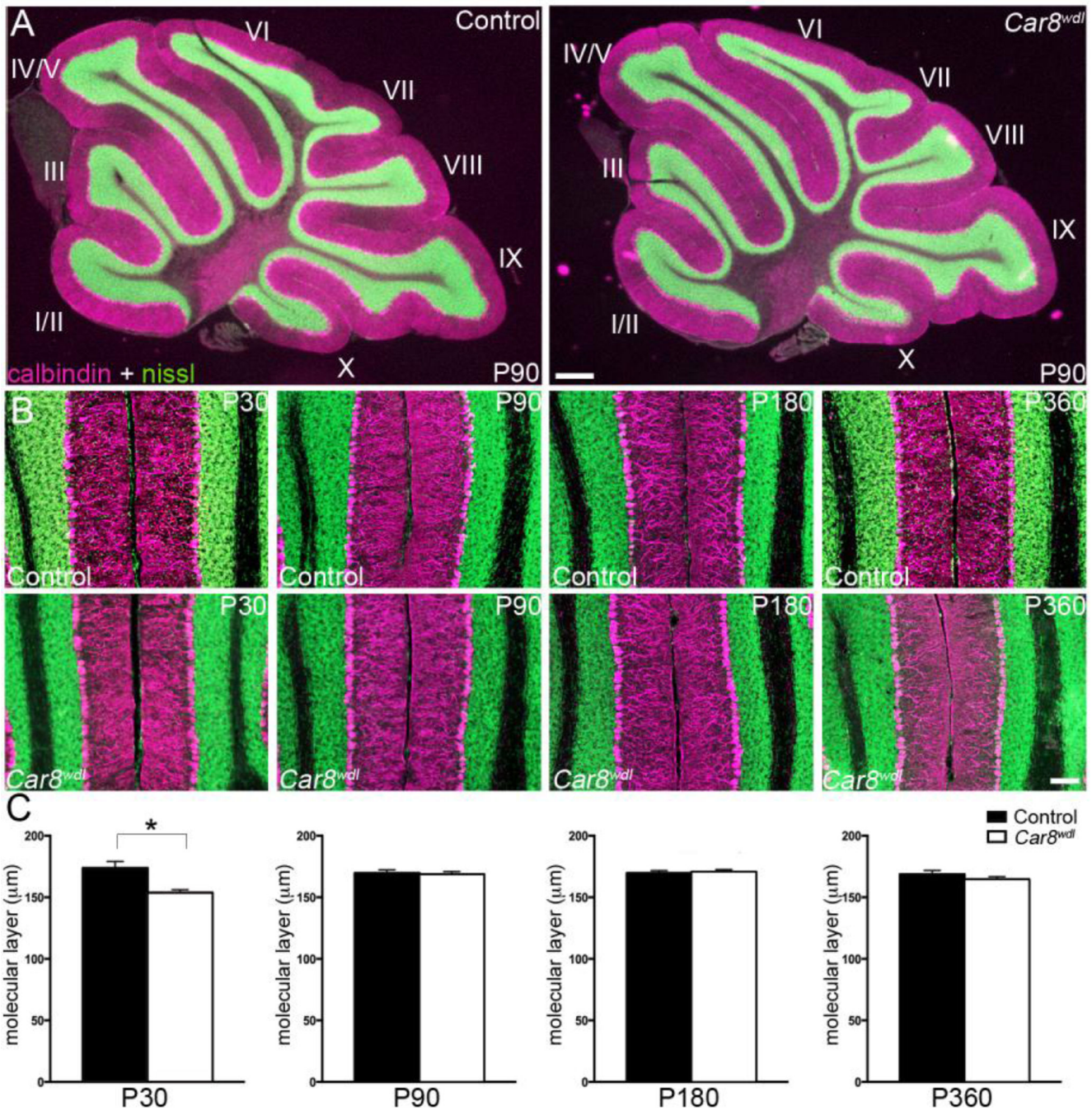

Figure 3. *Car8*^{wdl} mice do not exhibit Purkinje cell degeneration

The basic morphology of the cerebellum is not altered in *Car8*^{wdl} mice (A). The overall size of the cerebellum is normal and foliation is unaltered. Lobules are indicated with Roman numerals. Scale bar = 500 μm. *Car8*^{wdl} mice show no signs of Purkinje cell degeneration with age as determined by measuring the thickness of the molecular layer of the cerebellar cortex (B). Scale bar = 100 μm. Quantification of the measurements of molecular layer thickness at different ages only shows a significant difference at P30, suggesting a developmental delay (C, see text).

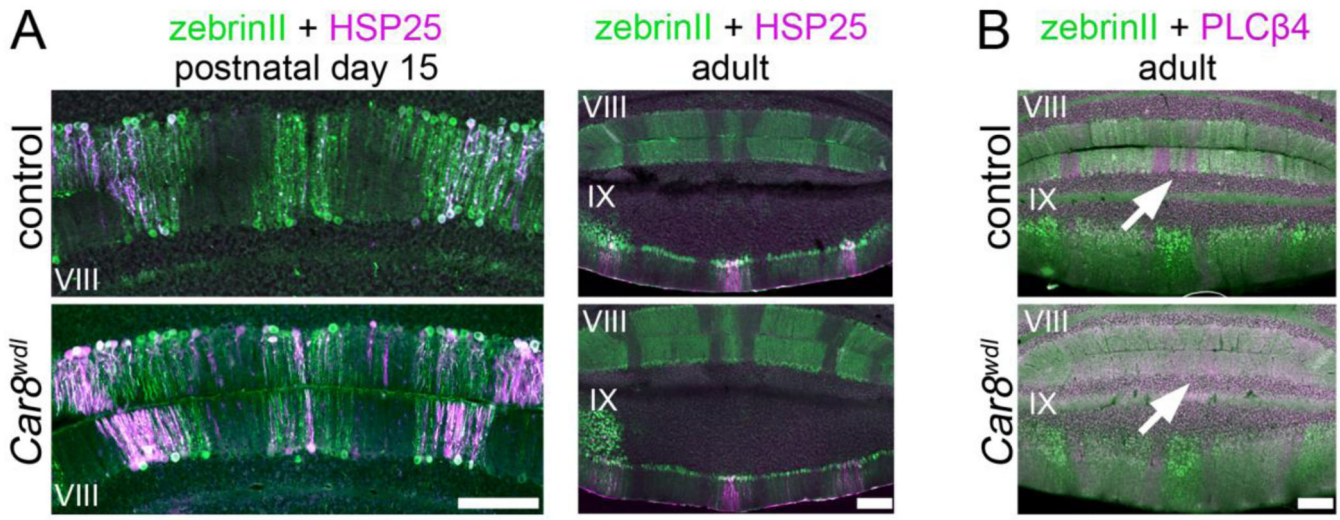

Figure 4. Purkinje cell zones are altered in *Car8*^{wdl} mice

The timing of when zebrinII and HSP25 zones occupy distinct territories is delayed in *Car8*^{wdl} mice (A). Scale bar = 150 μm. ZebrinII and PLCβ4 zonal boundaries are poorly delineated in adult *Car8*^{wdl} (B). Scale bar = 200 μm.

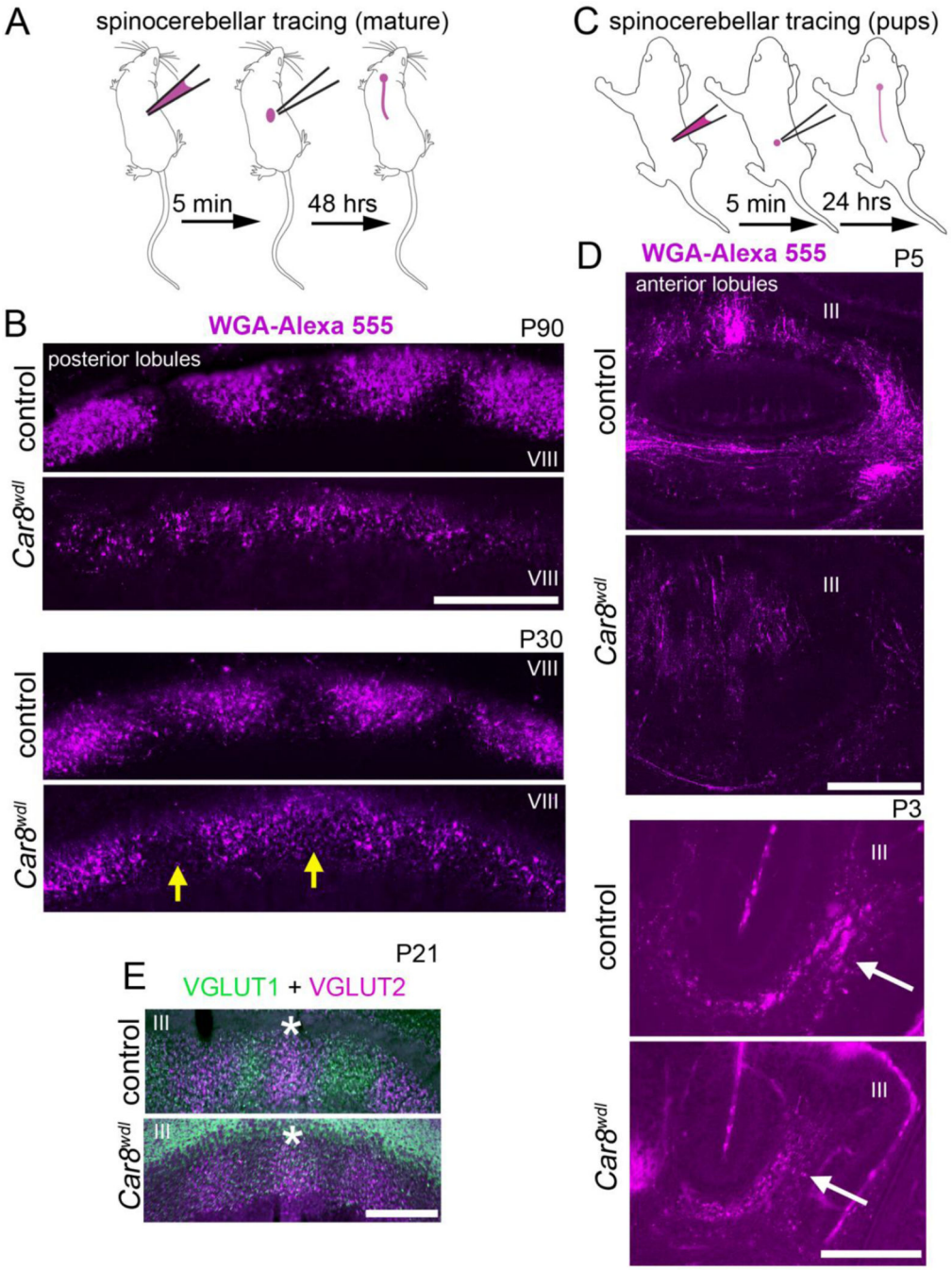

Figure 5. *Car8*^{wdl} mice have abnormally patterned circuit maps

Schematics illustrating the experimental paradigms for tracing spinocerebellar projections in adult (A) and early postnatal (C) mice. The pattern is less obvious at P90 compared to P30 (B). The yellow arrows point to weakly innervated domains in the mutant. Analysis of developing mice shows that mossy fiber topography is altered because the sensory pathways are incorrectly targeted and they weakly innervate the cerebellum during early postnatal development (D). The trajectory of perinatal spinocerebellar projections is preserved in P3 *Car8*^{wdl} mutants (D). Scale bar = 200 μm (juvenile P30 and adult P90) and 250 μm (pups).

Cuneocerebellar and spinocerebellar proprioceptive pathways exhibit overlapping domains in *Car8*^{wdl} mice as revealed by VGLUT1 and VGLUT2 expression (D). Scale bar = 500 μm.

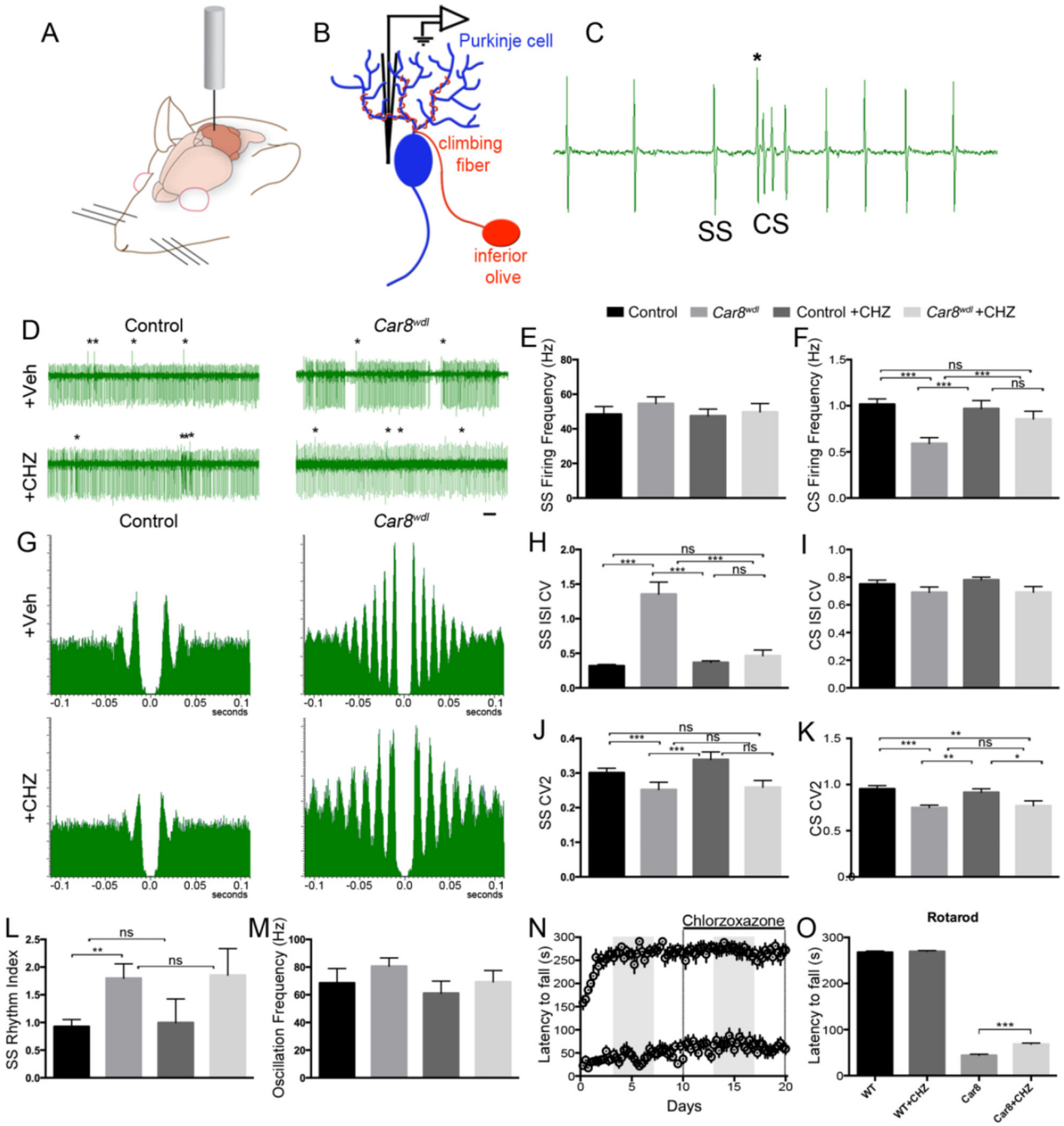

Figure 6. *Car8*^{wdl} Purkinje cell firing is abnormal *in vivo* and partially corrected by CHZ

A schematic of the *in vivo* recording setup. A metal electrode is lowered into a craniotomy opened over the cerebellum (A). A high power schematic of the recording setup. Extracellular action potential waveforms are used to examine Purkinje cell activity directly and inferior olive activity indirectly (B). A high power example of an extracellular recording of a Purkinje cell. The Purkinje cell fires both simple spikes (SS) and complex spikes (CS, labeled with asterisks), the latter is the response to activity of the climbing fibers that originate in the inferior olive (C). Example Purkinje cell recordings from control and

Car8^{wdl} mice with and without treatment with CHZ. Note the presence of large pauses only in untreated *Car8*^{wdl} mice (D). There is no significant difference in SS firing rate between any of the conditions (E). CS firing rate is significantly reduced in *Car8*^{wdl} mice as compared to all other conditions. CHZ treatment corrects CS firing rate in *Car8*^{wdl} mice (F). Example autocorrelograms of SS firing in control and *Car8*^{wdl} mice with and without treatment with CHZ. Peaks indicate more rhythmic firing (G). SS CV is significantly higher in *Car8*^{wdl} mice as compared to all other conditions. CHZ treatment corrects SS CV in *Car8*^{wdl} mice (H). CS CV is not significantly different between any of the conditions (I). SS CV2 is significantly lower in *Car8*^{wdl} mice as compared to control mice. SS CV2 is not corrected with CHZ treatment, as there is no significant difference between untreated and treated *Car8*^{wdl} mice (J). CS CV2 is significantly lower in *Car8*^{wdl} mice as compared to control mice. CS CV2 is also not corrected with CHZ treatment, as there is no significant difference between untreated and treated *Car8*^{wdl} mice (K). SS Rhythm index is significantly higher in *Car8*^{wdl} mice. This phenotype is not corrected with CHZ treatment, as there is no significant difference between untreated and treated *Car8*^{wdl} mice (L). There is no significant different in oscillation frequency between any of the conditions (M). Rotarod performance is significantly lower in *Car8*^{wdl} mice compared to control mice. Performance plateaued after 10 days of rotarod testing. The mice were treated with CHZ, which resulted in an increase in *Car8*^{wdl} performance and no change in the performance of controls (N). Although there is a significant increase in *Car8*^{wdl} performance after treatment with CHZ, the increase does not rise to the level of control mice (O).

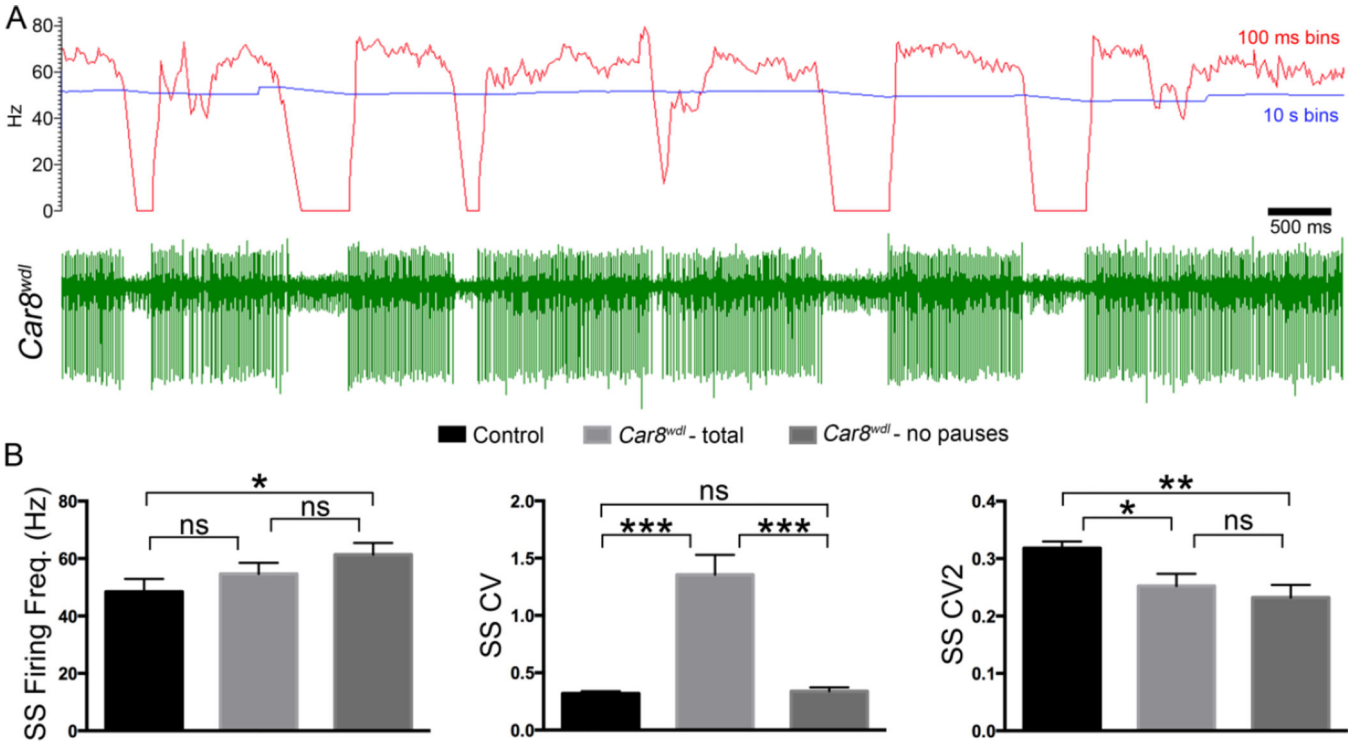

Figure 7. Long pauses in Purkinje cells firing cause an increase in irregularity in *Car8^{wdl}*

Raw trace of a Purkinje cell in *Car8^{wdl}* with the firing frequency binned into either 100 ms or 10 s bins (A). Longer bins mask the periods of quiescence. Firing frequency is increased when the pauses with lengths greater than or equal to two standard deviations above the average ISI are removed, but unchanged compared to control cells when the data are averaged over the entire trace including long pauses (B). Comparison of the mutant data to control cells in the absence of long pauses indicates that the higher CV (irregular firing) depends on the longer pauses (B). CV2 is lower in the mutant cells with and without the long pauses (B).

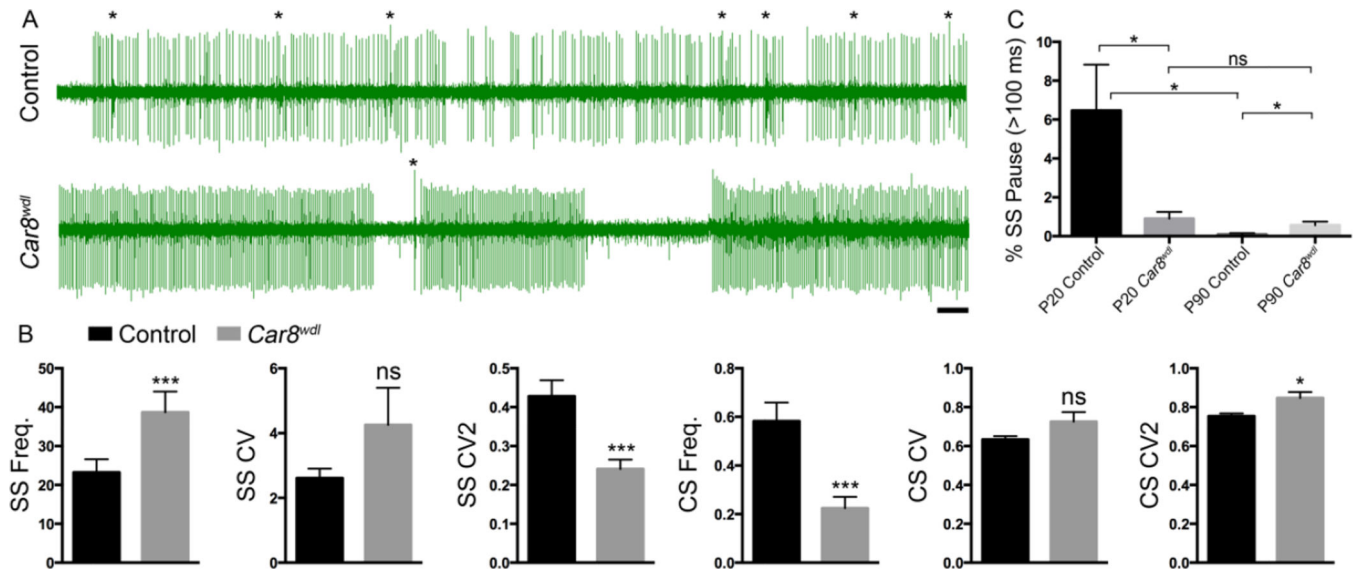

Figure 8. *Car8*^{wdl} Purkinje cells fire abnormally during development

Sample traces from control and *Car8*^{wdl} weanling mice demonstrate the irregular spiking in the control recording and the large pauses interrupting the regular firing in *Car8*^{wdl} mice. Complex spikes (CS) are indicated with asterisks (A). Scale bar = 500 ms. *Car8*^{wdl} mice fire SS at a significantly higher rate (B). Although highly variabile, *Car8*^{wdl} Purkinje cells trend toward a higher SS CV compared to controls. *Car8*^{wdl} Purkinje cells exhibit a significantly lower SS CV2 than controls. *Car8*^{wdl} Purkinje cells fire CS at a significantly lower rate than controls. There is no significant difference in CS CV between *Car8*^{wdl} and controls. However, there is a significant increase in CS CV2 in *Car8*^{wdl} mice. The percentage (%) of pauses over 100 ms is significantly lower in young *Car8*^{wdl} mice as compared to control Purkinje cells (C). However, when control mice reach adulthood, this percentage drops significantly. Age does not have a significant effect on % pauses in *Car8*^{wdl}.

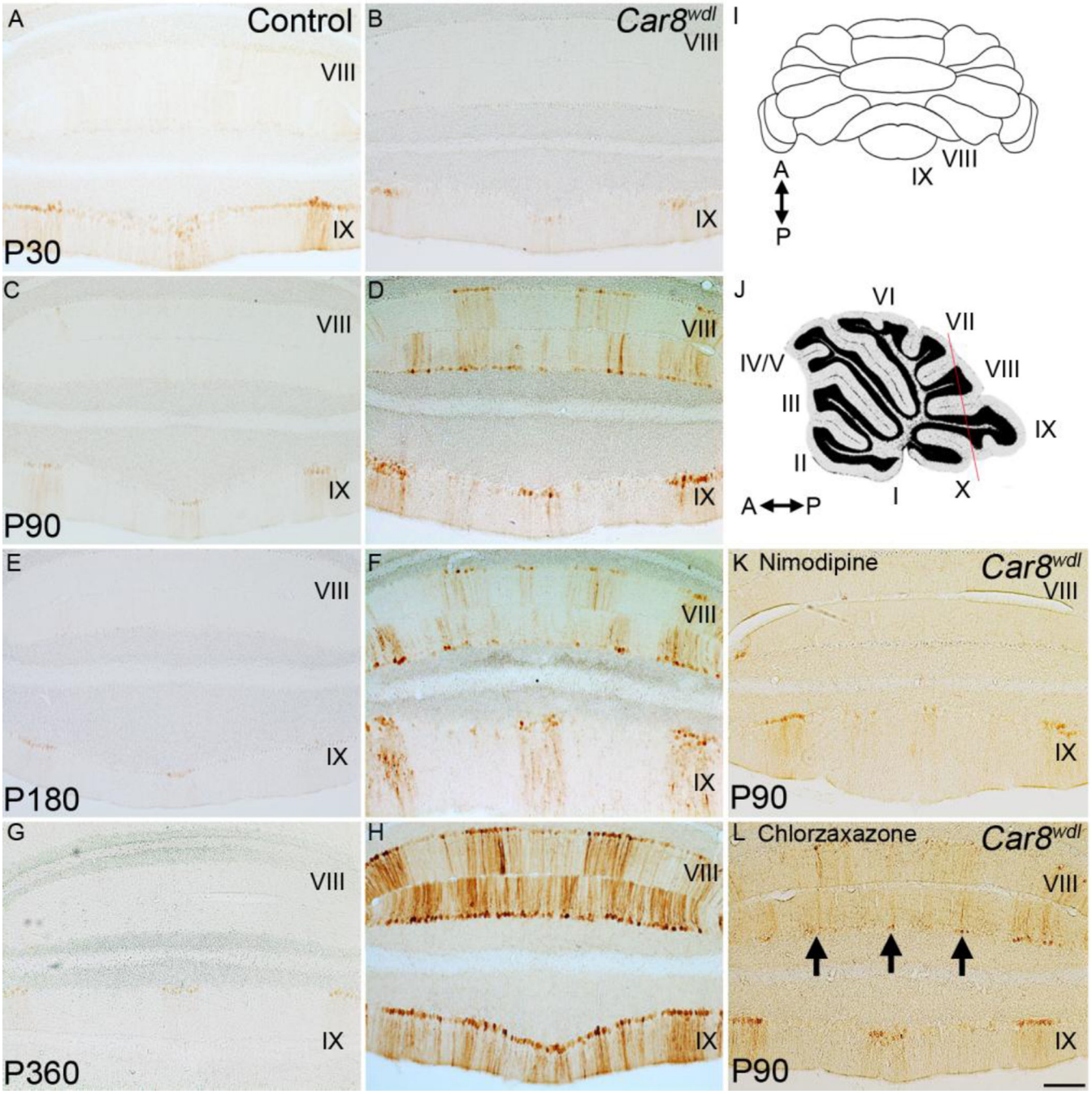

Figure 9. *Car8*^{wdl} cerebella exhibit a progressive spread of ectopic TH with age

TH is weakly expressed in a small subset of Purkinje cells in control P30 (A), P90 (C), P180 (E), and P360 (G) mice. In contrast, after P30 (B) in *Car8*^{wdl} TH is heavily expressed in distinct zones at P90 (D) and P180 (F), and by P360 the ectopic TH expressing cells predominate (H). Wholemount (I) and (J) sagittal schematics depicting the level from where the TH-stained tissue sections were acquired. *In vivo* nimodipine treatment lowers TH expression in P90 *Car8*^{wdl} mice (K). CHZ treatment at P90 had no detectable effect on

ectopic expression of TH in Purkinje cells (L). The arrows point to persistent TH expression. Scale bar = 200 μm (applies to all panels).